

Two-Pion-Exchange contributions to nucleon-nucleon interactions in covariant baryon chiral perturbation theory

Yang Xiao,¹ Chun-Xuan Wang,² Jun-Xu Lu,² and Li-Sheng Geng^{3,*}

¹*School of Physics, Beihang University, Beijing 100191,*

China & *Universit Paris-Saclay, CNRS/IN2P3, IJCLab, 91405 Orsay, France*

²*School of Physics, Beihang University, Beijing 100191, China*

³*School of Physics & Beijing Advanced Innovation Center for Big Data-based Precision Medicine, Beihang University, Beijing 100191, China. & School of Physics and Microelectronics, Zhengzhou University, Zhengzhou, Henan 450001, China*

Employing the covariant baryon chiral perturbation theory, we calculate the leading and next-to-leading order two-pion exchange (TPE) contributions to NN interactions up to order $O(p^3)$. We compare the so-obtained NN phase shifts of $2 \leq L \leq 6$ and mixing angles of $2 \leq J \leq 6$ with those obtained in the non-relativistic baryon chiral perturbation theory, which allows us to check the relativistic corrections to the middle-range part of NN interactions. We show that the contributions of relativistic TPE are more moderate than those of the non-relativistic TPE. The relativistic corrections play an important role in F-waves especially the 3F_2 partial wave. Moreover, the relativistic results seem to converge faster than the non-relativistic results in almost all the partial waves studied in the present work, consistent with the studies performed in the one-baryon sector.

PACS numbers:

I. INTRODUCTION

The nucleon-nucleon (NN) interaction is one of the most important inputs in nuclear physics and nuclear astrophysics. Since the seminal work of Yukawa [1], a variety of formulations of NN interactions have been proposed and thoroughly studied. Nowadays, a number of formulations of NN interactions, both phenomenological and more microscopic, are already of high precision, in the sense that they can describe NN scattering data with $T_{\text{Lab.}} < 350$ MeV with a $\chi^2/\text{d.o.f.} \approx 1$. In the phenomenological group, an accurate description of NN scattering data has been achieved by the Reid93 [2], Argonne V_{18} [3], and (CD-)Bonn potentials [4]. Although these phenomenological potentials work very well in describing the NN scattering data, there is no strong connection between these interactions and the underlying theory of the strong interaction, Quantum Chromodynamics (QCD). As for the microscopic ones, chiral effective field theory has achieved astonishing success. In the 1990s, Weinberg proposed that one can construct NN interactions using the Heavy Baryon (HB) chiral effective field theory (ChEFT) [5, 6]. Following this idea, numerous studies have been performed and the description of NN scattering data has become comparable to the phenomenological forces since 2003 [7–13]. In chiral NN interactions, the low energy constants (LECs) responsible for the short-range part of the NN interaction play an important role for the description of partial waves of $L \leq 2$ while two-pion and one-pion exchanges responsible for the middle and long-range parts, respectively, are important for and almost saturate higher partial waves [14]. Nonetheless, it was shown in Ref. [14] that a non-negligible discrepancy between chiral NN phase shifts and the Nejmegen partial wave analysis can still be observed in F-waves especially the 3F_2 and 3F_4 partial waves.

In a recent work [15], a study of NN interactions in covariant baryon chiral effective field theory was proposed. Interestingly, it was shown that the leading order (LO) relativistic NN interaction can describe the NN phaseshifts as well as the next-to-leading order (NLO) non-relativistic NN interaction. Of course, there is no mystery here because the covariant formulation can be viewed as a more efficient ordering of chiral expansion series. This can be seen from the fact that at LO the covariant formulation has four LECs¹ which is in between those of the LO and NLO non-relativistic ChEFT, two and nine, respectively. It remains to be seen whether relativistic effects or corrections are important in the two-pion exchange contributions. As there are no unknown LECs involved in these contributions, it should be more appropriate to check the relevance of relativistic corrections. More specifically, it would be interesting

*E-mail: lisheng.geng@buaa.edu.cn

¹ In fact, there are five LECs in Ref. [15], but according to the power counting of Ref. [16], there should be four, both of which provide very similar descriptions of the $J = 0$ and 1 partial wave phase shifts [17].

to investigate whether the F partial waves can be better described compared to Ref. [14]. Although in Ref. [14] a covariant calculation has been performed already, but the potentials are then expanded and only contributions up to the third order are kept. The corrections of higher order were neglected. We prefer not to do the non-relativistic expansion except for subtracting the power counting breaking (PCB) terms, so that all relativistic corrections are properly kept to maintain Lorentz invariance.

The main purpose of this work is to study the middle-range part of NN interactions, or more specifically, the two-pion exchange contributions in covariant baryon chiral effective field theory. In this work, we start from the covariant chiral πN Lagrangians up to second order [18] and construct the relativistic TPE potentials up to third order of chiral expansion. All power counting breaking terms are removed in the spirit of the extended-on-mass-shell scheme (EOMS) [19, 20], which has been well established in the one-baryon sector (see Ref. [21] for a short review). Then we calculate the NN T -matrix perturbatively with the constructed potentials and compute the phase shifts and mixing angles of $L \geq 2$ and $J \geq 2$.

The paper is organized as follows. In section II, the chiral Lagrangians needed for computing the two pion exchange contributions are briefly discussed. The TPE potentials up to third order are presented in section III. In section IV, we compare the so-obtained NN phase shifts with the Nijmegen partial wave analysis and those of Ref. [14]. A short summary and outlook is given in the last section.

II. CHIRAL LAGRANGIAN

First, we briefly explain the power counting rule in constructing the covariant baryon chiral Lagrangians, for more details, see, e.g., Refs. [19, 20]. The core of an effective field theory lies in the power counting rule, which emphasises the importance of certain Feynman diagrams for a given process. In this work we adopt the naive dimensional analysis, in which amplitudes are expanded in powers of (p/Λ_χ) , where p refers to the low energy scale including the three momentum of nucleons and the pion mass, Λ_χ refers to the chiral symmetry breaking scale. The chiral order ν of a Feynman diagram (after proper regularization) with L loops is defined as,

$$\nu = 4L - 2N_\pi - N_n + \sum_k kV_k, \quad (1)$$

where $N_{\pi,n}$ refers to the number of pion and nucleon propagators, and V_k donates the number of k -th order vertices. It was realized very early that such a definition is not full-filled in the one-baryon sector, because the large non-zero baryon mass at the chiral limit leads to the so-called power counting breaking problem [22]. Many approaches have been proposed to recover the power counting defined in Eq. (1), and the most studied ones are the heavy baryon formulation [23, 24], the infrared approach [25], and the extended-on-mass-shell approach [19, 20]. In the present work, we adopt the EOMS approach. The exact procedure of removing the PCB terms in the EOMS approach will be explained later.

In order to calculate the contributions of two-pion exchanges, we need the following LO and NLO πN Lagrangians,

$$\mathcal{L} = \mathcal{L}_{\pi N}^{(1)} + \mathcal{L}_{\pi N}^{(2)}, \quad (2)$$

where the superscript refers to the respective chiral order, and they read [18, 26], respectively,

$$\mathcal{L}_{\pi N}^{(1)} = \bar{N} \left(i \not{D} - m + \frac{g_A}{2} \not{u} \gamma_5 \right) N, \quad (3)$$

$$\mathcal{L}_{\pi N}^{(2)} = c_1 \langle \chi_+ \rangle \bar{N} N - \frac{c_2}{4m^2} \langle u^\mu u^\nu \rangle (D_\mu D_\nu + h.c.) + \frac{c_3}{2} \langle u^2 \rangle \bar{N} N - \frac{c_4}{4} \bar{N} \gamma^\mu \gamma^\nu [u_\mu, u_\nu] N, \quad (4)$$

where the nucleon field N is $N = (p, n)^T$, and the covariant derivative D is defined as $D_\mu = \partial_\mu + \Gamma_\mu$ with

$$\Gamma_\mu = \frac{1}{2} (u^\dagger \partial_\mu u + u \partial_\mu u^\dagger), \quad u = \exp \left(\frac{i\Phi}{2f_\pi} \right).$$

The pion field Φ is a 2×2 matrix of the following form,

$$\Phi = \begin{pmatrix} \pi^0 & \sqrt{2}\pi^+ \\ \sqrt{2}\pi^- & -\pi^0 \end{pmatrix},$$

and the axial current u_μ is defined as,

$$u_\mu = i (u^\dagger \partial_\mu u - u \partial_\mu u^\dagger),$$

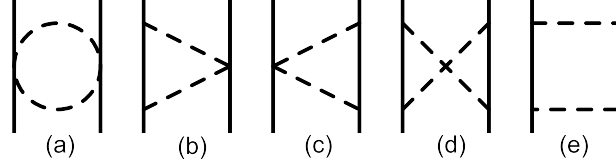


FIG. 1: Two pion exchange diagrams at $O(p^2)$. The pion nucleon vertices refer to vertices from $\mathcal{L}_{\pi N}^{(1)}$

TABLE I: Isospin factors of two-pion exchange diagrams at $O(p^2)$

	football	triangle L	triangle R	box	crossed
$I = 1$	$\frac{1}{8f_\pi^4}$	$-\frac{g_A^2}{8f_\pi^4}$	$-\frac{g_A^2}{8f_\pi^4}$	$\frac{g_A^4}{16f_\pi^4}$	$\frac{5g_A^4}{16f_\pi^4}$
$I = 0$	$-\frac{3}{8f_\pi^4}$	$\frac{3g_A^2}{8f_\pi^4}$	$\frac{3g_A^2}{8f_\pi^4}$	$\frac{9g_A^4}{16f_\pi^4}$	$-\frac{3g_A^4}{16f_\pi^4}$

where $\chi_+ = u^\dagger \chi u + u \chi u^\dagger$ with $\chi = \mathcal{M} = \text{diag}(m_\pi^2, m_\pi^2)$. The following values for the relevant LECs and masses are adopted in the numerical calculation: The pion decay constant $f_\pi = 92.4$ MeV, the axial coupling constant $g_A = 1.29$ [10]², the nucleon mass $m_n = 939$ MeV, the pion mass $m_\pi = 139$ MeV [27], and the low-energy constants $c_1 = -1.39$, $c_2 = 4.01$, $c_3 = -6.61$, $c_4 = 3.92$, all in units of GeV^{-1} , taken from Ref. [26]. One should note that the complete $\mathcal{L}_{\pi N}^{(2)}$ contains more terms than what are relevant here.

III. TWO PION EXCHANGE CONTRIBUTIONS

A. Leading order ($O(p^2)$) results

The two-pion exchange potentials are evaluated in the center-of-mass frame and at the isospin limit $m_u = m_d$. The leading order TPE diagrams are shown in Fig. 1. They contribute to order $O(p^2)$. All of them can be calculated directly in the EOMS scheme [19, 20], which is just the conventional dimensional regularization scheme with further removal of PCB terms. There is no so-called pinch singularity [5, 6, 14] in this case due to the appearance of the finite nucleon mass. Note that only direct diagrams need to be computed in the NN potential because of the Pauli exclusion principle [14]. In principle, the box diagram includes contributions from irreducible TPE and iterated OPE. The later originates from solving the scattering equation. However, since we treat the potentials perturbatively, there is no need to distinguish them. As a matter of fact, we also calculated the iterated OPE and found that the result is almost identical to that in Ref. [14]. For these reasons, the contributions from iterated OPE are not presented explicitly.

The complete TPE potentials are decomposed into the scalar integrals A_0, B_0, C_0 and D_0 multiplied with some polynomials and fermion bilinears using FeynCalc [28–30] and then calculated numerically with the help of OneLOop [31, 32]. However, there is still a tricky problem. That is, because of the large non-zero nucleon mass m_n in the chiral limit, lower order analytical terms may appear in higher order loop calculations which then break the naive power counting, namely the PCB problem [22]. The procedure to remove the PCB terms is rather standard and has been discussed in detail in Refs. [19–21, 33]. At the end, the total TPE potentials at $O(p^2)$ take the following form,

$$V_{TPE}^{(2)} = \sum_i N_i V_i^{(2)}, \quad (5)$$

where i refers to the i -th Feynman diagram contributing at this order, N_i donates the isospin factor which is summarized in Table I, $V_i^{(2)}$ refers to the potential of each Feynman diagram and

$$V_i^{(2)} = V_i'^{(2)} - V_i''^{(2)}, \quad (6)$$

² This choice is made in order to be consistent with Refs. [7–13]. Using the more standard value $g_A = 1.267$ yields almost identical results.

where $V_i'^{(2)}$ denotes the total potential and $V_i''^{(2)}$ is the PCB term. The total potentials for the football, triangle, cross and box diagrams read explicitly

$$\begin{aligned}
V_{\text{Football}}'^{(2)} &= -\frac{B_4 [3 (4m_\pi^2 - t) B_0 (t, m_\pi^2, m_\pi^2) + 6A_0 (m_\pi^2) + 12m_\pi^2 - 2t]}{288\pi^2}, \\
V_{\text{TrigL}}'^{(2)} &= \frac{2m_n^2 \{(B_5 + B_6) m_n [2 (2f_1 + f_2 + f_3) + C_0 (A)] + 2B_4 f_4\} + B_4 f_5}{8\pi^2}, \\
V_{\text{TrigR}}'^{(2)} &= V_{\text{TrigL}}'^{(2)} (B_5 \mapsto B_7, B_6 \mapsto B_8), \\
V_{\text{Cross}}'^{(2)} &= -\frac{1}{16\pi^2} \{2m_n^2 \{m_n [2 (B_5 + B_6 + B_7 + B_8) (f_2 + f_3) + 4 (4B_3 m_n + B_5 + B_6 + B_7 + B_8) f_1 \\
&\quad + (4B_3 m_n + B_5 + B_6) C_0 (A) + (4B_3 m_n + B_7 + B_8) C_0 (B)] + 4 \{B_4 f_4 + m_n^2 [(B_5 + B_6 + B_7 + B_8) \\
&\quad \times D_{22} m_n + D_{23} (2B_3 m_n^2 + B_9 + B_{10}) + 2B_4 D_{00}] \} + 2B_3 B_0 (t, m_\pi^2, m_\pi^2) \} + B_4 f_5\}, \\
V_{\text{Box}}'^{(2)} &= -\frac{1}{16\pi^2} \{2m_n^2 \{m_n [-2 (B_5 + B_6 + B_7 + B_8) (f_2 + f_3) - 4 (-4B_3 m_n + B_5 + B_6 + B_7 + B_8) f_1 \\
&\quad + (4B_3 m_n - B_5 - B_6) C_0 (A) + (4B_3 m_n - B_7 - B_8) C_0 (B)] - 4B_4 f_4 + 4m_n^2 [-(B_5 + B_6 + B_7 + B_8) \\
&\quad \times D_{22} m_n + D_{23} (2B_3 m_n^2 + B_9 + B_{10}) - 2B_4 D_{00}] \} + 2B_3 B_0 (t, m_\pi^2, m_\pi^2) - B_4 f_5\},
\end{aligned} \tag{7}$$

with

$$\begin{aligned}
f_1 &= \text{PaVe} (1, \{m_n^2, t, m_n^2\}, \{m_n^2, m_\pi^2, m_\pi^2\}), \\
f_2 &= \text{PaVe} (1, 1, \{m_n^2, t, m_n^2\}, \{m_n^2, m_\pi^2, m_\pi^2\}), \\
f_3 &= \text{PaVe} (1, 2, \{m_n^2, t, m_n^2\}, \{m_n^2, m_\pi^2, m_\pi^2\}), \\
f_4 &= \text{PaVe} (0, 0, \{m_n^2, t, m_n^2\}, \{m_n^2, m_\pi^2, m_\pi^2\}), \\
f_5 &= \text{PaVe} (0, 0, \{t\}, \{m_\pi^2, m_\pi^2\}), \\
C_0(A) &= C_0 (m_n^2, m_n^2, t, m_\pi^2, m_n^2, m_\pi^2), \\
C_0(B) &= C_0 (m_n^2, t, m_n^2, m_n^2, m_\pi^2, m_\pi^2),
\end{aligned} \tag{8}$$

where $D_{i,j}$ and PaVe are the library functions in FeynCalc and can be simplified to the scalar integrals A_0, B_0, C_0, D_0 , and B_{3-10} donate the following fermion bilinears,

$$\begin{aligned}
B_3 &= \bar{u}(\mathbf{p}') u(\mathbf{p}) \bar{u}(-\mathbf{p}') u(-\mathbf{p}), \\
B_4 &= \bar{u}(\mathbf{p}') \gamma^\mu u(\mathbf{p}) \bar{u}(-\mathbf{p}') \gamma_\mu u(-\mathbf{p}), \\
B_5 &= \bar{u}(\mathbf{p}') \not{p}_2 u(\mathbf{p}) \bar{u}(-\mathbf{p}') u(-\mathbf{p}), \\
B_6 &= \bar{u}(\mathbf{p}') \not{p}_4 u(\mathbf{p}) \bar{u}(-\mathbf{p}') u(-\mathbf{p}), \\
B_7 &= \bar{u}(\mathbf{p}') u(\mathbf{p}) \bar{u}(-\mathbf{p}') \not{p}_1 u(-\mathbf{p}), \\
B_8 &= \bar{u}(\mathbf{p}') u(\mathbf{p}) \bar{u}(-\mathbf{p}') \not{p}_3 u(-\mathbf{p}), \\
B_9 &= \bar{u}(\mathbf{p}') \not{p}_2 u(\mathbf{p}) \bar{u}(-\mathbf{p}') \not{p}_1 u(-\mathbf{p}), \\
B_{10} &= \bar{u}(\mathbf{p}') \not{p}_4 u(\mathbf{p}) \bar{u}(-\mathbf{p}') \not{p}_1 u(-\mathbf{p}),
\end{aligned} \tag{9}$$

where \mathbf{p}, \mathbf{p}' are incoming and outgoing momentum, $p_1^\mu = (E, \mathbf{p})$, $p_2^\mu = (E, -\mathbf{p})$, $p_3^\mu = (E', \mathbf{p}')$, $p_4^\mu = (E', -\mathbf{p}')$, $E = \sqrt{\mathbf{p}^2 + m_n^2}$, $E' = \sqrt{\mathbf{p}'^2 + m_n^2}$, $t = (p_1 - p_3)^2$, $u(p)$ and $\bar{u}(p)$ are Dirac spinors,

$$u(\mathbf{p}) = N \left(\frac{\mathbb{1}}{\sigma \cdot \mathbf{p}} \right) \chi_s, \quad N = \sqrt{\frac{E + m_n}{2m_n}}, \tag{10}$$

where χ_s donates the pauli spinor matrix and σ is the pauli matrix. To obtain the PCB terms, it is convenient to project the potential from momentum space to helicity space so that the potentials become scalars without the pauli matrix and can easily be expanded in powers of small parameters. The detailed procedure to do this projection is explained later. However, because of their complexity, we do not show the explicit expressions of V' in helicity

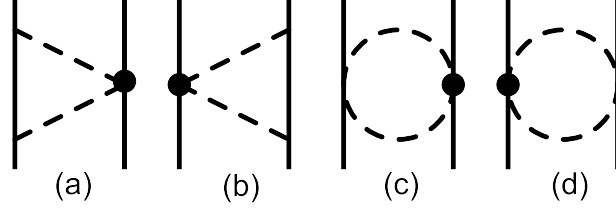


FIG. 2: Two pion exchange diagrams at $O(p^3)$. The black dots denote vertices from $\mathcal{L}_{\pi N}^{(2)}$

space here. One thing to be noted is that although the above bilinears appear to break parity symmetry, e.g. $B_9 \xrightarrow{\text{Parity}} \bar{u}(\mathbf{p}') \not{p}_4 u(\mathbf{p}) \bar{u}(-\mathbf{p}') \not{p}_3 u(-\mathbf{p}) \neq B_9$, they do not. This can be easily shown utilizing momentum conservation and the Dirac equation, i.e.

$$\begin{aligned}
 B_9 &= \bar{u}(\mathbf{p}') \not{p}_2 u(\mathbf{p}) \bar{u}(-\mathbf{p}') \not{p}_1 u(-\mathbf{p}) \\
 &= \bar{u}(\mathbf{p}') \frac{1}{2} (\not{p}_2 + \not{p}_3 - \not{p}_1 + \not{p}_4) u(\mathbf{p}) \bar{u}(-\mathbf{p}') \frac{1}{2} (\not{p}_1 + \not{p}_4 - \not{p}_2 + \not{p}_3) u(-\mathbf{p}) \\
 &= \frac{1}{4} \bar{u}(\mathbf{p}') (\not{p}_2 + \not{p}_4) u(\mathbf{p}) \bar{u}(-\mathbf{p}') (\not{p}_1 + \not{p}_3) u(-\mathbf{p}) \\
 &\xrightarrow{\text{Parity}} B_9.
 \end{aligned}$$

The PCB terms in helicity space read,

$$\begin{aligned}
 V_{\text{Football}}^{(2)} &= 0, \\
 V_{\text{TrigL}}^{(2)} &= \frac{H_1 m_n^2 \ln\left(\frac{\mu}{m_n}\right)}{4\pi^2}, \\
 V_{\text{TrigR}}^{(2)} &= V_{\text{TrigL}}^{(2)}, \\
 V_{\text{Cross}}^{(2)} &= \frac{H_1 m_n^2 \left[3 \ln\left(\frac{\mu}{m_n}\right) - 1\right]}{4\pi^2}, \\
 V_{\text{Box}}^{(2)} &= \frac{H_1 m_n^2 \left[\ln\left(\frac{\mu}{m_n}\right) - 1\right]}{4\pi^2},
 \end{aligned} \tag{11}$$

where $\mu = 1\text{GeV}$ refers to the renormalization scale, and H_1 is,

$$H_1 = \left[|\bar{\lambda}_1 + \lambda_1| \cos\left(\frac{\theta}{2}\right) + |\bar{\lambda}_1 - \lambda_1| \sin\left(\frac{\theta}{2}\right) \right] \left[|\bar{\lambda}_2 + \lambda_2| \cos\left(\frac{\theta}{2}\right) - |\bar{\lambda}_2 - \lambda_2| \sin\left(\frac{\theta}{2}\right) \right], \tag{12}$$

where $\lambda_{1,2}, \bar{\lambda}_{1,2}$ denote the helicities of incoming, outgoing particles respectively and θ refers to the scattering angle.

B. Next-to-leading order ($O(p^3)$) results

The next-to-leading order TPE diagrams are shown in Fig. 2. These diagrams are the same as the corresponding diagrams shown in Fig. 1 with the replacement of the πN vertices $\mathcal{L}_{\pi N}^{(1)}$ with $\mathcal{L}_{\pi N}^{(2)}$. Note that there is no box diagram or cross diagram at this order because there is no πNN vertex at order $O(p^2)$.

The next-to-leading order TPE potentials read,

$$V_{TPE}^{(3)} = V_{\text{FootballL}}^{(3)} + V_{\text{FootballR}}^{(3)} + V_{\text{TrigL}}^{(3)} + V_{\text{TrigR}}^{(3)}, \tag{13}$$

where the notation is the same as that stated above. The isospin factors have been included in the potential V at this order for simplicity.

$$V_{\text{FootballL}}^{(3)} = \frac{(3 - 4I)c_4(-2B_4m_n + B_7 + B_8)[3(t - 4m_\pi^2)B_0(t, m_\pi^2, m_\pi^2) - 6A_0(m_\pi^2) + 2(t - 6m_\pi^2)]}{1152\pi^2 f_\pi^4}, \quad (14)$$

$$V_{\text{FootballR}}^{(3)} = V_{\text{FootballL}}^{(3)}(B_7 \rightarrow B_5, B_8 \rightarrow B_6),$$

where $I = 0, 1$ refers to the isospin. The football diagrams have no PCB term, and the explicit expressions of the triangle potentials at this order are not given explicitly due to their complexity³

In order to compute the phase shifts, we need to transform the potentials into LSJ basis where L is the total orbital angular momentum, S is the total spin, and J is the total angular momentum. The procedure to project potentials from momentum space to LSJ space is rather standard [34, 35]. Here we refer to Ref. [35] for more details. At first, we compute the potentials directly in momentum space. Then, we transfer them to helicity basis. Next, they are rotated to the total angular momentum space $|JM\rangle$ using the Wigner d-functions. Last, they are projected to LSJ basis. In order to compute the phase shifts and mixing angle, we follow the procedure of Ref. [36],

$$\delta_{LSJ} = -\frac{m_n^2 |\mathbf{p}|}{16\pi^2 E} \text{Re}\langle LSJ | \mathcal{T}_{NN} | LSJ \rangle, \quad (15)$$

$$\epsilon_J = \frac{m_n^2 |\mathbf{p}|}{16\pi^2 E} \text{Re}\langle J - 1, 1, J | \mathcal{T}_{NN} | J + 1, 1, J \rangle.$$

where $\mathcal{T}_{NN} = V_{NN}$. Note that the kinematical prefactors here differ from those of Ref. [14] because of convention.

IV. RESULTS AND DISCUSSIONS

In this section, the phase shifts of $2 \leq L \leq 6$ and mixing angles of $2 \leq J \leq 6$ in the relativistic framework are presented and compared with those of the non-relativistic calculations of Ref. [14].

A. D-wave

The D-wave phase shifts and mixing angle ϵ_2 are shown in Fig. 3. For all the cases the chiral NN phase shifts are in good agreement with data up to $T_{\text{lab}} = 50$ MeV, and the relativistic results show the same tendency as their non-relativistic counterparts, but the TPE contributions are more moderate, so for all the D-waves the relativistic results are in better agreement with the Nijmegen phase shifts perhaps with the exception of $^3\text{D}_1$ for $T_{\text{lab}} \leq 200$ MeV⁴, where both descriptions show a much stronger u-turn shape, inconsistent with data. The non-relativistic result for $^3\text{D}_1$ is in fair agreement with data up to $T_{\text{lab}} = 200$ MeV due to the cancellation of irreducible TPE and iterated OPE [14], while in the relativistic case, the contribution of the irreducible part is moderate so that the curve shifts downwards. The mixing angle ϵ_2 in the relativistic method is in better agreement with data due to the same reason. Although the relativistic corrections are sizeable in D-wave and improve the description of data, the still relatively large discrepancy indicates the need of short-range contributions, namely the contact potentials controlled by LECs.

A few words are in order for the convergence pattern. For the coupled channels, because of the cancellation of the irreducible part and the iterated part in the leading order TPE, the contribution of the next-to-leading order TPE is very large compared with that of the leading order TPE. But for the singlet channel $^1\text{D}_2$, contrast to our expectation, the iterated part contributes negligibly to the phase shifts while the next-to-leading order TPE contributes a lot. Moreover, the contribution of the next-to-leading order TPE seems to be larger than the contribution of OPE. All in all, although the relativistic results are quantitatively better than the non-relativistic results, pion-exchange contributions alone are not enough to explain the D-wave data, as concluded in Ref. [14].

³ They could be obtained as a Mathematica notebook from the authors upon request.

⁴ For the $^3\text{D}_1$ partial wave, the relativistic results in fact agree better with data than their non-relativistic counterparts for the whole energy region shown in Fig. 3.

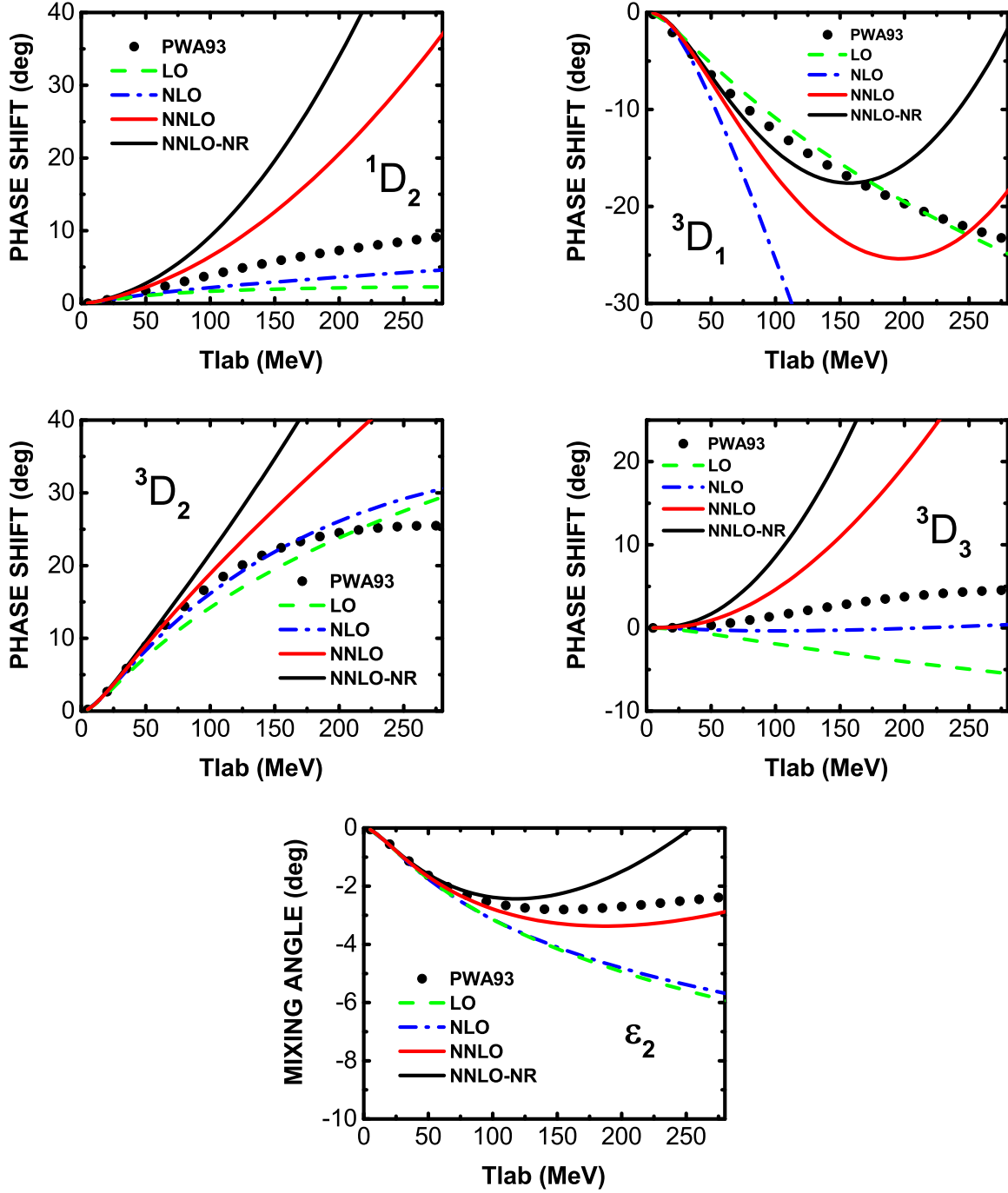


FIG. 3: D-wave phase shifts and mixing angle ϵ_2 as a function of T_{lab} . The black dots refer to the Nijmegen partial wave phase shifts [37]. The green dashed curves correspond to the contributions from relativistic OPE [15], the blue dash dotted curves represent the contributions of TPE at second order, the red solid curves contain the next-to-leading order TPE while the black curves are their non-relativistic counterparts [14] with g_A fixed at 1.29.

B. F-wave

The F-wave phase shifts and mixing angle are depicted in Fig. 4. As in the D-wave case, the relativistic TPE is moderate so that overall the phase shifts are in better agreement with data. For the 1F_3 partial wave, the relativistic results are almost identical to data up to $T_{\text{lab}} = 230$ MeV. For the 3F_3 partial wave, the relativistic phase shifts are slightly better than the non-relativistic ones. For the 3F_4 partial wave, the two results are almost identical. However, for the 3F_2 partial wave, the contributions of relativistic TPE are opposite to those of the non-relativistic case which leads to a fair agreement with data for the largest T_{lab} shown in this Figure. In addition, the fact that the contributions of leading order relativistic TPE are relatively small indicates a good convergence at least up to $O(p^2)$. The contributions of the next-to-leading order TPE are a bit large for the 3F_3 and 3F_4 partial waves when $T_{\text{lab}} \geq 150$ MeV. This may not be too surprising because for this energy, the momentum transfer q is already about $3.85m_\pi \approx 530$ MeV and therefore may not be regarded as a good low energy scale.

C. G-wave

The G-wave phase shifts and mixing angle are depicted in Fig. 5. Again, for almost all the cases the relativistic phase shifts are in better agreement with data with the exception of 3G_3 , where the non-relativistic results are slightly better. For the 1G_4 , 3G_4 , 3G_5 and ϵ_4 partial waves, the relativistic calculations are almost identical to data up to $T_{\text{lab}} = 280$ MeV. For the 3G_3 partial waves, the relativistic phase shift is also in perfect agreement with data up to $T_{\text{lab}} = 200$ MeV. Moreover, the fact that the contributions of relativistic TPE are quite small demonstrates a proper convergence pattern in this partial wave.

D. H-wave

The H-wave phase shifts and mixing angle are depicted in Fig. 6. For the H wave, although the TPE contributions are much smaller, the relativistic corrections still improve the description of data. For the 1H_5 , 3H_4 , 3H_5 , the relativistic and non-relativistic phase shifts are almost indistinguishable. Only for 3H_6 , the contribution of the next-to-leading order TPE seems to be a bit large when $T_{\text{lab}} \geq 150$ MeV.

E. I-wave

The I-wave phase shifts and mixing angle are depicted in Fig. 7. The relativistic phase shifts are nearly identical to the non-relativistic phase shifts and are in perfect agreement with data for this partial wave due to the negligible contribution of TPE. Notice that for the 3I_7 partial wave, the Nijmegen partial wave phase shifts [37] are larger than those in Ref. [38].

V. SUMMARY AND OUTLOOK

Based on the covariant πN Lagrangians, we constructed the relativistic TPE potentials up to $O(p^3)$. Treating these potentials perturbatively, we further calculated the chiral NN phase shifts of $2 \leq L \leq 6$ and mixing angles of $2 \leq J \leq 6$ and then compared our results with those of the non-relativistic expansion. We found that for all the partial waves the contributions of relativistic TPE are more moderate than their non-relativistic counterparts and therefore the obtained NN phase shifts are in better agreement with the Nijmegen partial wave analysis than the non-relativistic results [14] especially for the F partial waves. Moreover, we showed that the large discrepancies between the non-relativistic phase shifts and data in the 3F_2 partial wave can be eliminated by including the relativistic corrections. But for the 3F_4 partial wave, the relativistic corrections are insignificant. We demonstrated that the relativistic method converges faster for the partial waves with $L \geq 3$. However, we also found that the contributions of relativistic TPE at the next-to-leading order, similar to their non-relativistic counterparts, are a bit large in $^3(J+1)_J$ partial waves when $T_{\text{lab}} \geq 150$ MeV, which indicates that the perturbation theory up to $O(p^3)$ may not work well in this energy region.

To summarize, although relativistic corrections are found to improve the description of data as expected, they are not significant enough to alter the results of Ref. [14] at least at a qualitative level, thus supporting all the existing studies using the non-relativistic two-pion exchange contributions of Ref. [14] as inputs. On the other hand, given the

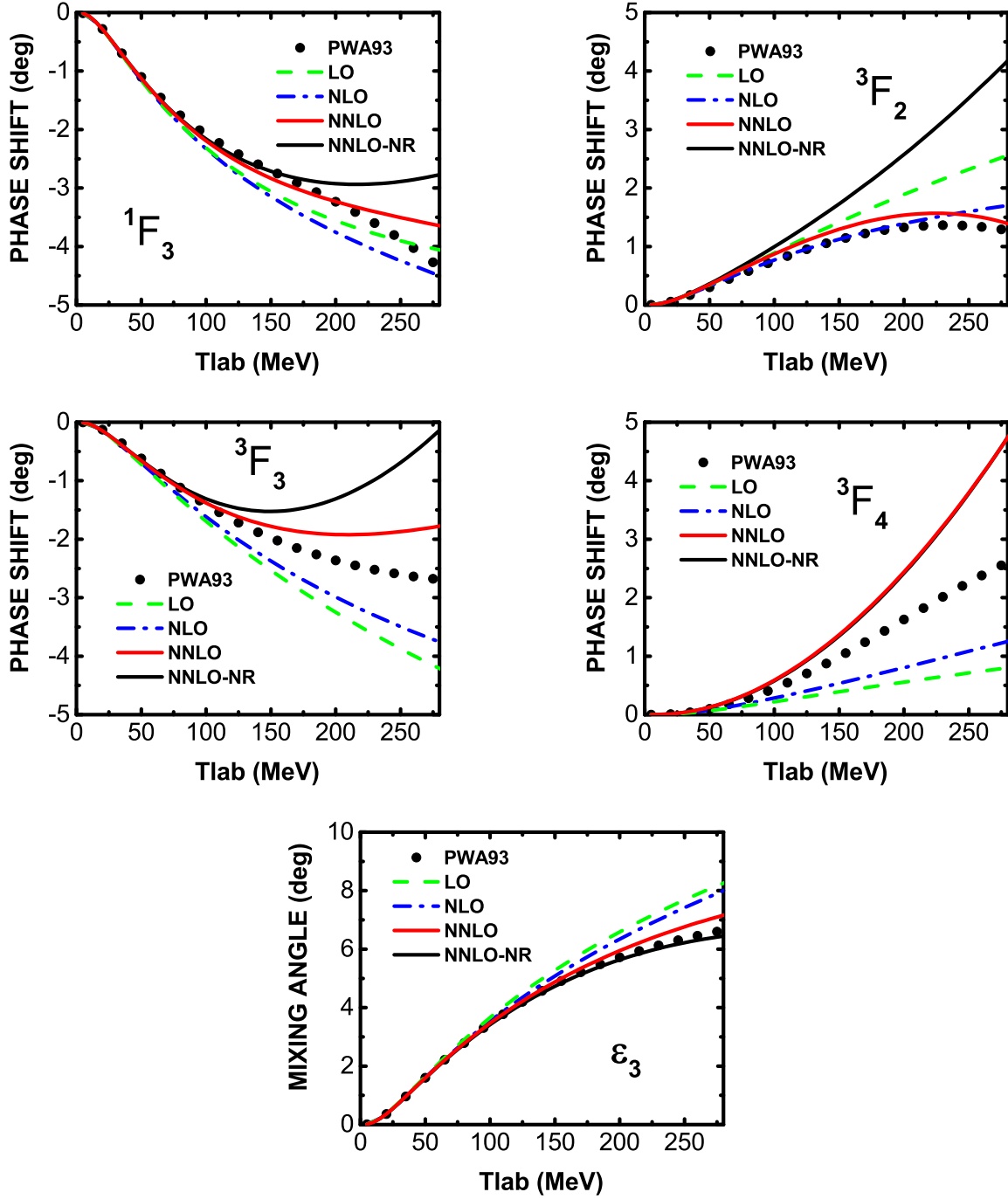


FIG. 4: Same as Fig. 3, but for F-wave phase shifts and mixing angle ϵ_3 .

covariant nature of the two-pion exchanges presented in this work, they can be easily utilized in the recent series of works [15–17, 39–43] which need such two-pion exchanges as inputs and their relevance in such settings remain to be explored.

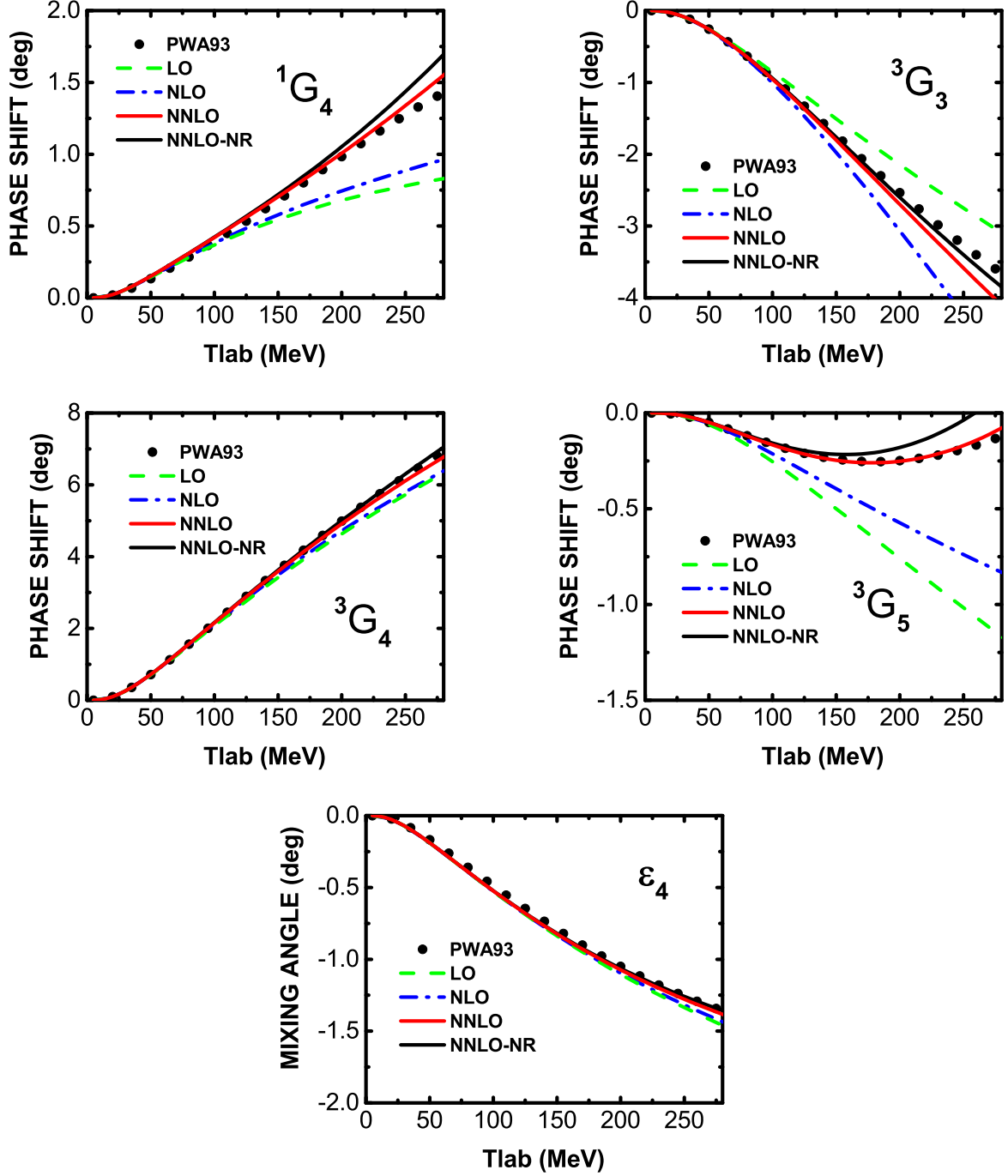


FIG. 5: Same as Fig. 3, but for G-wave phase shifts and mixing angle ϵ_4 .

VI. ACKNOWLEDGEMENTS

Yang Xiao thanks Ubirajara L. van Kolck for useful discussions. This work is supported in part by the National Natural Science Foundation of China under Grants Nos.11735003, 11975041, and 11961141004. Yang Xiao acknowledges

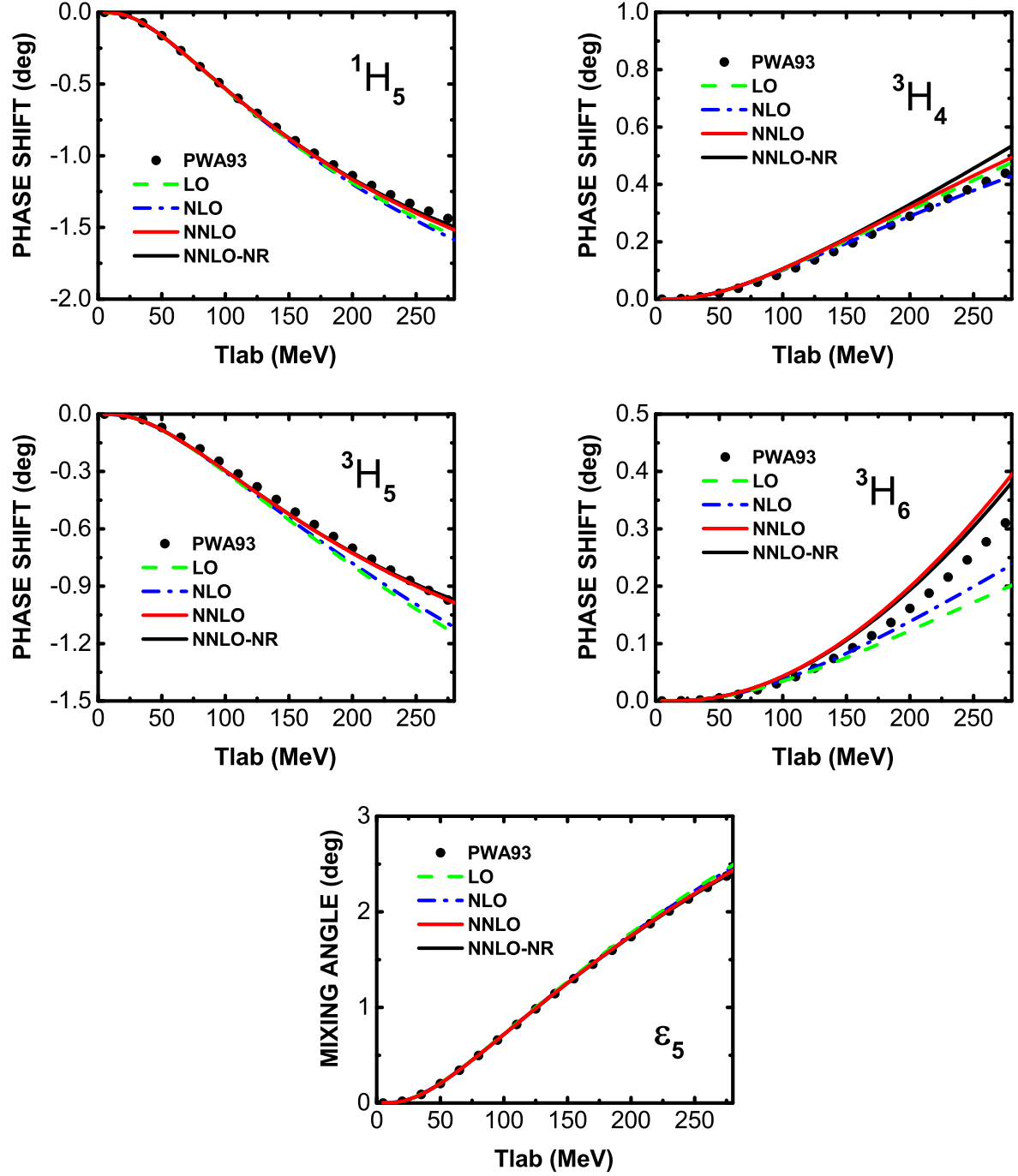


FIG. 6: Same as Fig. 3, but for H-wave phase shifts and mixing angle ϵ_5 .

the support from China Scholarship Council.

-
- [1] H. Yukawa, Proc. Phys. Math. Soc. Jap. **17** (1935) 48 [Prog. Theor. Phys. Suppl. **1** 1].
 - [2] V. G. J. Stoks, R. A. M. Klomp, C. P. F. Terheggen and J. J. de Swart, Phys. Rev. C **49** (1994) 2950
 - [3] R. B. Wiringa, V. G. J. Stoks and R. Schiavilla, Phys. Rev. C **51** (1995) 38
 - [4] R. Machleidt, Phys. Rev. C **63** (2001) 024001

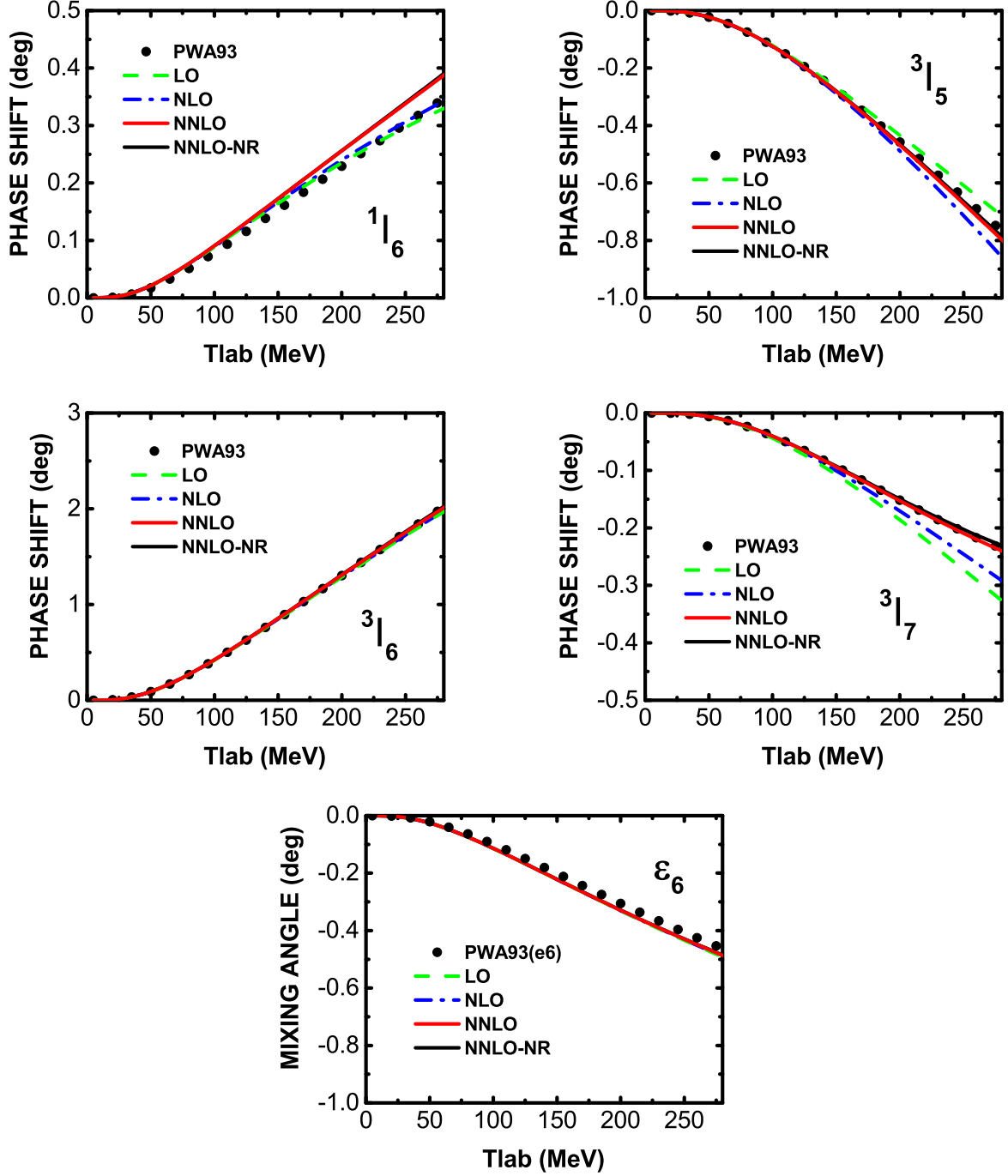


FIG. 7: Same as Fig. 3, but for I-wave phase shifts and mixing angle ϵ_6 .

- [5] S. Weinberg, Phys. Lett. B **251** (1990) 288.
- [6] S. Weinberg, Nucl. Phys. B **363** (1991) 3.
- [7] D. R. Entem and R. Machleidt, Phys. Rev. C **68** (2003) 041001
- [8] E. Epelbaum, W. Glockle and U. G. Meissner, Nucl. Phys. A **747** (2005) 362
- [9] E. Epelbaum, H. W. Hammer and U. G. Meissner, Rev. Mod. Phys. **81** (2009) 1773
- [10] R. Machleidt and D. R. Entem, Phys. Rept. **503** (2011) 1
- [11] E. Epelbaum, H. Krebs and U. G. Meißner, Phys. Rev. Lett. **115** (2015) no.12, 122301
- [12] D. R. Entem, N. Kaiser, R. Machleidt and Y. Nosyk, Phys. Rev. C **92** (2015) no.6, 064001
- [13] D. R. Entem, R. Machleidt and Y. Nosyk, Phys. Rev. C **96** (2017) no.2, 024004

- [14] N. Kaiser, R. Brockmann and W. Weise, Nucl. Phys. A **625** (1997) 758
- [15] X. L. Ren, K. W. Li, L. S. Geng, B. W. Long, P. Ring and J. Meng, Chin. Phys. C **42** (2018) no.1, 014103
- [16] Y. Xiao, L. S. Geng and X. L. Ren, Phys. Rev. C **99** (2019) no.2, 024004
- [17] C. X. Wang, L. S. Geng and B. Long, [arXiv:2001.08483 [nucl-th]].
- [18] N. Fettes, U. G. Meissner, M. Mojzis and S. Steininger, Annals Phys. **283** (2000) 273
- [19] J. Gegelia and G. Japaridze, Phys. Rev. D **60** (1999) 114038
- [20] T. Fuchs, J. Gegelia, G. Japaridze and S. Scherer, Phys. Rev. D **68** (2003) 056005
- [21] L. Geng, Front. Phys. (Beijing) **8**, 328-348 (2013)
- [22] J. Gasser, M. E. Sainio and A. Svarc, Nucl. Phys. B **307** (1988), 779-853
- [23] E. E. Jenkins and A. V. Manohar, Phys. Lett. B **255** (1991), 558-562
- [24] V. Bernard, N. Kaiser, J. Kambor and U. G. Meissner, Nucl. Phys. B **388** (1992), 315-345
- [25] T. Becher and H. Leutwyler, Eur. Phys. J. C **9** (1999), 643-671
- [26] Y. H. Chen, D. L. Yao and H. Q. Zheng, Phys. Rev. D **87** (2013) 054019
- [27] M. Tanabashi *et al.* [Particle Data Group], Phys. Rev. D **98** (2018) no.3, 030001.
- [28] V. Shtabovenko, R. Mertig and F. Orellana, Comput. Phys. Commun. **256** (2020), 107478
- [29] V. Shtabovenko, R. Mertig and F. Orellana, Comput. Phys. Commun. **207** (2016), 432-444
- [30] R. Mertig, M. Bohm and A. Denner, Comput. Phys. Commun. **64** (1991), 345-359
- [31] A. van Hameren, C. G. Papadopoulos and R. Pittau, JHEP **09** (2009), 106
- [32] A. van Hameren, Comput. Phys. Commun. **182** (2011), 2427-2438
- [33] J. X. Lu, L. S. Geng, X. L. Ren and M. L. Du, Phys. Rev. D **99** (2019) no.5, 054024
- [34] K. Erkelenz, R. Alzetta and K. Holinde, Nucl. Phys. A **176** (1971) 413.
- [35] K. Erkelenz, Phys. Rept. **13** (1974) 191.
- [36] J. Gasser and U. G. Meissner, Phys. Lett. B **258** (1991), 219-224
- [37] V. G. J. Stoks, R. A. M. Klomp, M. C. M. Rentmeester and J. J. de Swart, Phys. Rev. C **48** (1993), 792-815
- [38] R. A. Arndt, J. S. Hyslop, III and L. D. Roper, Phys. Rev. D **35** (1987), 128
- [39] K. W. Li, X. L. Ren, L. S. Geng and B. W. Long, Chin. Phys. C **42**, no.1, 014105 (2018)
- [40] X. L. Ren, K. W. Li, L. S. Geng and J. Meng, [arXiv:1712.10083 [nucl-th]].
- [41] J. Song, K. W. Li and L. S. Geng, Phys. Rev. C **97**, no.6, 065201 (2018)
- [42] K. W. Li, T. Hyodo and L. S. Geng, Phys. Rev. C **98**, no.6, 065203 (2018)
- [43] Q. Q. Bai, C. X. Wang, Y. Xiao and L. S. Geng, [arXiv:2007.01638 [nucl-th]].